Received: 8 January 2024 | Revised: 22 March 2024 | Accepted: 16 May 2024

DOI: 10.1002/sia.7337

NOTES AND INSIGHTS

SURFACE and INTERFACE ANALYSIS WILEY

Surface science insight note: Imaging X-ray photoelectron spectroscopy

Vincent Fernandez[1] | Neal Fairley[2] | David Morgan[3,4] | Pascal Bargiela[5] | Jonas Baltrusaitis[6]

[1]Nantes Université, CNRS, Institut des Matériaux Jean Rouxel, IMN, Nantes, France

[2]Casa Software Ltd, Teignmouth, Devon, UK

[3]School of Chemistry, Translational Research Hub, Cardiff University, Cardiff, UK

[4]HarwellXPS – EPSRC National Facility for Photoelectron Spectroscopy, Research Complex at Harwell (RCaH), Didcot, Oxon, UK

[5]Universite de Pau et des Pays de l'Adour, E2S UPPA, CNRS, IPREM, Pau, France

[6]Department of Chemical and Biomolecular Engineering, Lehigh University, Bethlehem, Pennsylvania, USA

Correspondence
Jonas Baltrusaitis, Department of Chemical and Biomolecular Engineering, Lehigh University, 111 Research Drive, Bethlehem, PA 18015, USA.
Email: job314@lehigh.edu

Funding information
U.S. Department of Energy, Office of Science, Basic Energy Sciences, Grant/Award Number: DE-SC0012577; CNRS, Grant/Award Number: 1317144

Quantification of X-ray photoelectron spectroscopy (XPS) data is often limited by the heterogeneous nature of the material surface. However, it is often the case that heterogeneous material contains areas within the analyzed area that are effectively homogeneous. In this *Insight* note, concepts, and methods used to analyze both XPS data are presented to extract both spatial and spectral information from heterogeneous surfaces. These concepts and methods are applied to a specific material surface that contains three chemical compounds separated spatially. The analysis entails converting XPS image data to spectral data and is designed to highlight the potential of XPS imaging in revealing compositional information correlation with spatial information. Properties of algorithms used to evaluate XPS images and spectra are described to outline their application to image data. A case study of an imaging XPS data set is presented that demonstrates how poor signal-to-noise images, where the signal is recorded for 4 s per image, are still open to analysis yielding useful information. Ultimately, the methods presented here will aid in interpreting complex XPS data obtained from spatially complex materials often obtained during extensive cycling, such as conventional or electrocatalysts.

KEYWORDS
heterogeneous, imaging, PCA, signal-to-noise, XPS

1 | INTRODUCTION

Most experiments performed by X-ray photoelectron spectroscopy (XPS) involve the acquisition of spectra. Spectra measured by XPS are acquired from a specific analysis area. For most spectra, the analysis area is relatively large in microscopy terms, because one factor in obtaining signal-to-noise sufficient for data analysis is the size of the analysis area. The problem in using a large analysis area arises if the sample is heterogeneous. Determining relationships between atoms by XPS is confused by large-area analysis of heterogeneous materials. Hence, spectra acquired at the limits of spatial resolution for XPS are desirable. Unfortunately, spectra acquired at the micron level are deficient in signal. However, if many spectra are acquired at micron spatial resolution, then there is the possibility of recovering spectral information with signal-to-noise sufficient for the analysis of heterogeneous samples. Imaging XPS is a means of acquiring spatially resolved spectra and therefore provides a solution to the XPS of heterogeneous materials.

Photoemission spectra are measured from an analysis area defined by either an X-ray probe size or an area defined by the transfer lens column of an XPS instrument.[1] If quantitative information is the target of analysis,[2] the assumption that permits the conversion of spectroscopic data to elemental composition is that the material from which the signal is collected is homogeneous. The homogeneity of the

material is essential for several reasons. One important reason is related to the ability of an instrument to maintain an analysis area constant in size and position during the acquisition of spectra. An instrument for which the transmission response to variation in kinetic energy is not constant may suffer from issues associated with alterations in the analysis area when measuring spectra.[3] The second reason is that, differences in composition over the analysis area, yield spectra that are difficult to interpret without a full knowledge of the sample. Thus, for heterogeneous materials, measuring the XPS signal from a range of locations makes it possible to find regions where materials are nearly homogeneous. When presented with a heterogeneous sample, imaging a sample of unknown composition represents a systematic approach to acquiring spatially resolved spectra. Consequently, commercial instruments manufactured by Kratos Analytical Ltd, ThermoFisher Scientific, Ulvac PHI Inc., Focus GmbH, or Scienta-Omicron AB routinely include options aimed at measuring spectra at selected locations on a sample that map changes in composition. In addition, commercially available instruments include stigmatic imaging of a sample (Kratos Analytical Ltd, ThermoFisher Scientific, and Focus GmbH), where the transfer lens column forms a total-energy image of the analysis area before the hemispherical analyzer, which in turn focuses an energy-resolved stigmatic image of the analysis area on a two-dimensional detector. While spatial resolution for XPS is poorer than other imaging techniques, such as electron microscopy, there are sufficient instances where the need to co-localize spatial and elemental information warrants the use of imaging XPS.[4] Therefore, this *Insight* note presents technical details of use to those wishing to explore how imaging XPS is used in practice.

Techniques and mathematical background that make chemical state analysis by imaging XPS possible are reviewed herein. A case study of imaging XPS data is used to illustrate analysis techniques that recover spectra from image data sets.

1.1 | Imaging XPS data acquisition considerations

There are three approaches to generating XPS images as shown in Figure 1. In particular, (A) Kratos dual analyzer spherical mirror stigmatic imaging configuration corresponds to one of them. Both the lower hemispherical analyzer, designed to measure spectra, and the upper spherical mirror energy analyzer make use of the same electron optics for the transfer lens column. Apertures in the transfer lens column allow spectra from the selected area of the sample to be acquired via the lower HSA, while energy-specific stigmatic images acquired via the top analyzer are used to create imaging XPS data. In (B) ThermoFisher Scientific Fourier transform lens stigmatic configuration is shown. Sigmatic images and spectra are acquired using the same HSA. Spectra are acquired using channeltron detectors arranged to accommodate a two-dimensional image detector. In (C) Ulvac Phi scanned micron-focused X-ray probe is shown. Pixels are defined by the X-ray spot on the sample, from which a spectrum per pixel is acquired. The data set consists of many spatially resolved spectra; therefore, an image of the sample at each energy can be constructed from these spectra.

When a probe in the form of a focused beam of X-rays is used to define a relatively small area of the sample from which a recorded signal emanates, the probe area on the sample from which the photoemission signal is recorded defines the spatial resolution of an image. At each location on the sample defined by the probe, a spectrum is recorded. An image is constructed from a raster of the probe, where the raster traces out a rectangular area of dimensions larger than the probe area. The other approach to measuring image data is the direct measurement of an image, making use of electron optics, to form for a given energy, an image of the sample on a two-dimensional detector. Image data is recorded as a two-dimensional set of data bins. A sequence of images is collected where each image is measured at an energy, incremented between image measurements. A data set constructed by these means allows the construction of spectra by gathering signals from images into data bins that depend on energy only. Both approaches to imaging XPS form data sets in which data bins are arranged over three dimensions representing increments in x, y, and energy. Data sets constructed from either approach to imaging XPS are mathematically and physically equivalent.

The need to obtain higher spatial resolution during imaging XPS analysis necessarily implies reduced signal intensity per image pixel. A typical imaging XPS experiment involves scanning both energy and

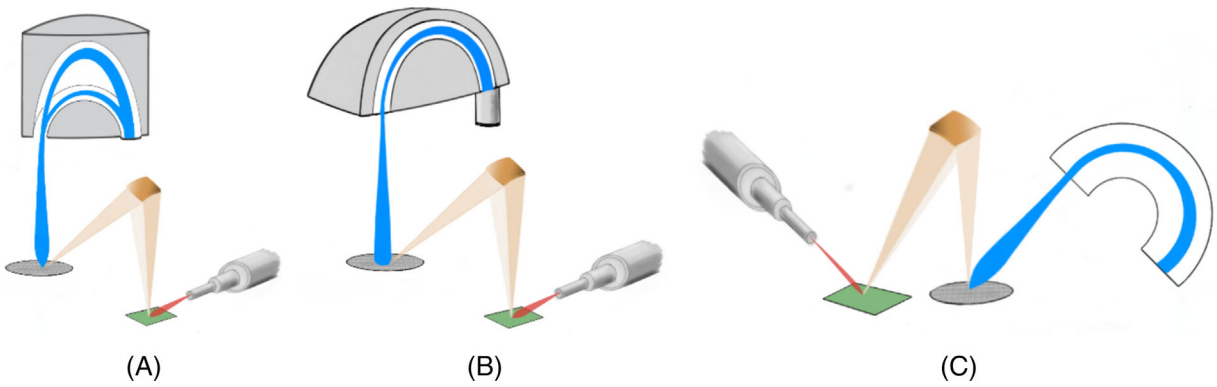

FIGURE 1 Three different instruments designed to create images of a sample.

location. Hence, XPS images can be partitioned into three-dimensional data sets. Each data bin records a signal, which is assigned two coordinates that define the position within the analysis area, while a third coordinate specifies the energy. Partitioning the signal in such a manner results in poor signal-to-noise in any given data bin, but the total image or a total spectrum contains a good signal-to-noise for the accumulated data. The reason for the high quality of these summed forms of data lies in the time over which imaging XPS experiments are performed. Imaging XPS experiments with good signal-to-noise for each pixel are long compared to other spectroscopic measurements. Therefore, data processing becomes an important part of imaging XPS since it requires noise reduction by principal component analysis (PCA) to allow for shorter acquisition times. In particular, PCA allows for the transformation of data and interpretation of mathematical results in the context of sample properties and is based on a singular value decomposition (SVD).[5–7] This *Insight* note aims to allow an informed use of PCA in the analysis of XPS data sets. Therefore, these mathematical aspects of PCA in the form of SVD are presented herein. A case study of an imaging XPS data set presented in this work allows aspects of data processing to be examined in the context of a sample for which large-area analysis otherwise yields confusing quantification by XPS. Results in the form of PCA-computed images are used to extract spectra representative of different spatial domains within the analysis area. Quantification of a spectrum identified with one domain demonstrates the principles behind the quantification of heterogeneous materials.

1.2 | Further considerations of imaging XPS data processing

The target of imaging XPS is constructing spectra from specific areas on the sample and then applying standard quantification techniques based on the integration of regions and peak models to understand sample surface chemistry.[8–14] Since spectra associated with locations on a sample may be of poor-quality signal-to-noise, the first steps in data processing are designed to enhance signal by numerical methods based on linear algebra. Imaging XPS data sets formed from spectra or images can be treated identically. In linear algebra terms, spectra and images are one-dimensional vectors. The only difference between spectra and images occurs with respect to the number of coordinates within a vector formed from a spectrum or an image. In other words, computing an SVD value for data in either spectral or imaging form yields identical results. However, from a computational perspective, the time required can be significantly different. The CPU time of a computer required to compute the SVD for a set of vectors depends on the algorithm in use but also depends on the dimension size for vectors formed from spectra or images. The easiest way to appreciate the computational problem is to understand that underlying SVD is the need to formulate a covariance matrix for a set of vectors. A covariance matrix is a square symmetric matrix of dimension equal to the number of vectors used in the construction. An image data set defined with 128×128 pixels contains 16,384 spectra. The same imaging XPS data set may contain as few as 100 images. The covariance matrix constructed from these 100 images would be of dimension size 100×100, which is significantly more manageable than a covariance matrix of dimension $16{,}384 \times 16{,}384$ formed from spectra. Due to the mathematical equivalence between vectors formed from spectra or images in terms of SVD, it is possible to choose, from an imaging data set, the most advantageous vectors for computational efficiency. Algorithms such as iterative SVD (iSVD) (described below) in CasaXPS[15] or non-linear iterative partial least squares (NIPALS)[16] do not require the formation of a covariance matrix explicitly, but any algorithm that computes all eigenvalues and eigenvectors of the covariance matrix must choose the smaller dimensioned covariance matrix.

The output from PCA is sometimes more interesting when presented in image form than in spectral form. The advantage of working with images rather than spectra is that images, after transformation by PCA, highlight spatial information for a sample which in some cases can be used to extract spectra with a common chemistry simply by classifying image pixels by intensity. Ultimately, spectra that can be associated with zones on a sample of different compositions are the objective for XPS, but the analysis of images provides a path for identifying the ideal scenario of spatially resolved spectra. A further point relating to PCA of imaging XPS data sets is how PCA results are presented in practice. It has already been noted that imaging XPS provides two alternative sources for vectors used in SVD. The terms scores and loading[16] are often used to describe the output of PCA. However, in the case of imaging XPS, the meaning of scores and loading changes depending on the chosen type of vector, for example, whether vectors are formed from either images or spectra. If the results of PCA are recognized as vectors and one form of these output vectors is described in terms of images or spectra, then these results are readily viewed as abstract images (AI) or abstract spectra (AS) with physical significance. AI offer spatial variations within the data set, while AS can be related to changes in peak and background within spectra. AI or AS representing noise are also easily identified. However, if described in terms of scores and loading, these two outputs from PCA change meaning depending on the chosen form for the input vectors. Therefore, in this *Insight* note, PCA outputs will be described as AI, AS, or generically as abstract factors (AF).

1.3 | iSVD algorithm

iSVD[17,18] is a simple but effective iterative method for computing PCA AFs in the order of significance. As described in this *Insight*, iSVD is founded on a least squares principle, and it is this principle that places the covariance matrix at the heart of any mathematical explanations relating to PCA. However, SVD is more than simply a means of constructing AFs ranked by significance with respect to the original set of vectors. SVD is a mathematical decomposition with a useful purpose; specifically, SVD provides a robust numerical means of computing a linear least squares (LLS) fit of vectors to a chosen vector.[19] SVD and the rapid computation of eigenvalues and eigenvectors of a

covariance matrix is a tool that underpins both linear and nonlinear (Marquardt–Levenberg[20]) optimization, both of which are essential tools for the analysis of XPS data.

The input to iSVD is a set of data vectors and the number of desired AFs is an output from the iSVD algorithm. When computing AFs, iSVD does not explicitly form the covariance matrix. However, logically the iterative steps of iSVD transform the covariance matrix formed from the input vectors. Each AF computed by iSVD causes changes in all vectors involved in the calculation. Thus, in computing the set of AFs, a set of vectors is maintained from which it is possible to construct a covariance matrix. The properties of the covariance matrix are a guide to how iSVD processes AFs. For this reason, Figure 2 is a set of covariance matrices constructed by iSVD from a set of valence band spectra measured from vanadium foil. The covariance matrix corresponding to the initial data is labeled *Valence Band*. Matrix elements of a covariance matrix are equal to the dot product of vectors. Therefore, a covariance matrix formed from data vectors includes nonzero off-diagonal matrix elements. Subsequent applications of iSVD requesting the calculation of one, two, three, five, and 10 AF create sets of vectors from which covariance matrices are formed. These covariance matrices are presented by coloring the matrix elements to reflect the magnitude and sign of the dot product between vectors for a given output from iSVD. The color scale, used to display vector output from iSVD, is chosen to assign black to matrix elements that are close to zero. Hence, the black horizontal and vertical lines of matrix elements indicate the dot product between a computed AF, and all other vectors, for the specified number of AFs, are close to zero. Figure 2 graphically illustrates how vectors are transformed by iSVD. If all AFs were computed by iSVD, then the only nonzero matrix elements of the covariance matrix would appear along the leading diagonal of the covariance matrix formed from a complete set of AFs. Increasing from one to 10 the number of AFs results in the patterns shown in Figure 2, where the colors for off-diagonal matrix elements darken, while the diagonal matrix elements brighten in the yellow color. The brightness of matrix elements indicates the success of gathering information through computing a given number of AFs.

The definition of SVD is as follows. Given a set of data vectors $\{\boldsymbol{d}_1,\boldsymbol{d}_2,\boldsymbol{d}_3,\cdots,\boldsymbol{d}_m\}$, $\boldsymbol{d}_i \in \mathbb{R}^n$, the standard procedure for expressing these vectors as a corresponding set of AFs $\{\boldsymbol{u}_1,\boldsymbol{u}_2,\boldsymbol{u}_3,\cdots,\boldsymbol{u}_m\}$ is through Equation 1.

$$\boldsymbol{D} = \boldsymbol{U}\boldsymbol{W}\boldsymbol{V}^T, \tag{1}$$

where the matrices in Equation 1 are defined in terms of an eigenanalysis to include, $\boldsymbol{D} = [\boldsymbol{d}_1,\boldsymbol{d}_2,\boldsymbol{d}_3,\cdots,\boldsymbol{d}_m]$, $\boldsymbol{U} = [\hat{\boldsymbol{u}}_1,\hat{\boldsymbol{u}}_2,\hat{\boldsymbol{u}}_3,\cdots,\hat{\boldsymbol{u}}_m]$, $\boldsymbol{u}_i \in \mathbb{R}^n$, $\boldsymbol{W}$ is a diagonal matrix with diagonal matrix elements equal to the square root of the eigenvalues of the *covariance matrix* defined by Equation 2, and $\boldsymbol{V}$ is the matrix formed from the normalized eigenvectors of $\boldsymbol{Z}$, ordered with respect to the square root of eigenvalues to correlate with the diagonal matrix $\boldsymbol{W}$

$$\boldsymbol{Z} = \boldsymbol{D}^T\boldsymbol{D}. \tag{2}$$

The covariance matrix Equation 2 is therefore central to the mathematics of SVD. Equation 1 and Equation 2 underpin the iSVD algorithm.

These eigenvectors are computed by sequentially transforming the set of vectors using 3×3 matrices calculated from three vectors

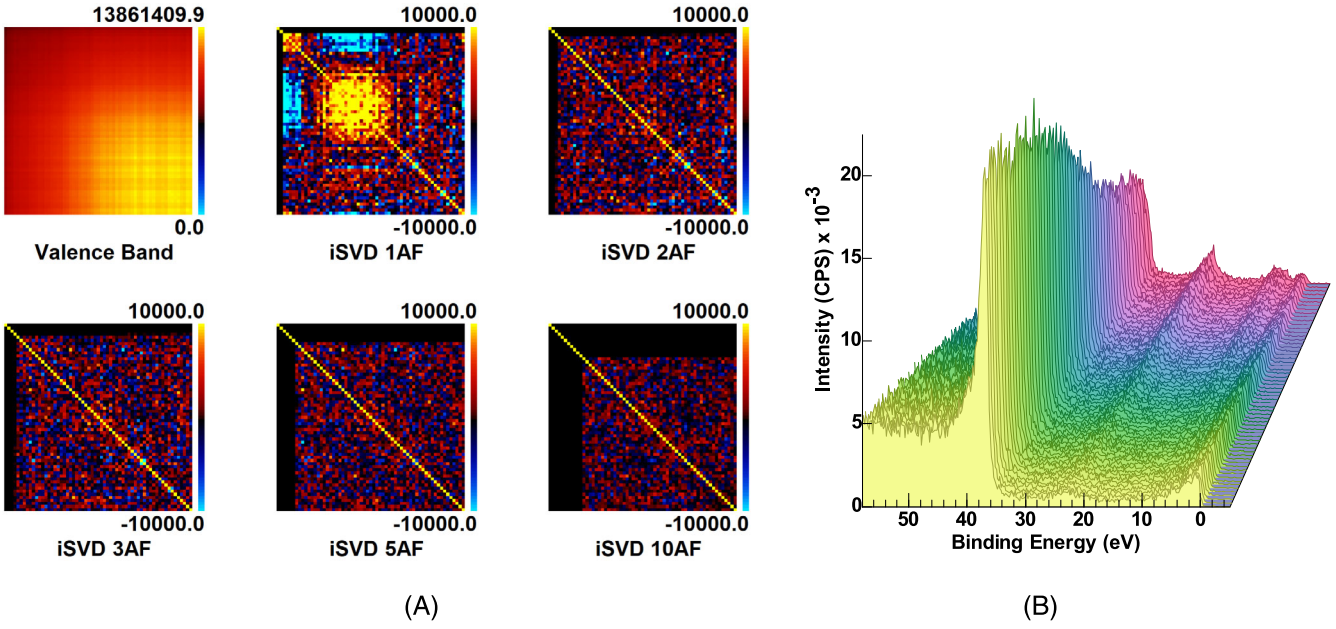

FIGURE 2 (A) Image representation of covariance matrices formed from a set of vectors in the unprocessed state (labeled as valence band) and various applications of iterative SVD (iSVD) requesting the computation of 1, 2, 3, 5, and 10 AFs from the unprocessed data. (B) Spectra used to compute AFs used to construct the covariance matrices in (A). These spectra are measured from a vanadium foil representing an extended valence band region spanning from 60 to 0 eV to include V 3p, O 2 s and signal close to the Fermi edge of vanadium metal.

at a time. The process is an iterative procedure where after each pass through the data set an approximation to the next largest eigenvector is obtained. The steps are defined in Table 1:

These simple steps in Table 1 provide a regime for computing the AF vectors for a data matrix. Each such step places the AF corresponding to the largest eigenvalue of the 3×3 covariance matrix in the vector $\boldsymbol{y_1}$.

The algorithm in Table 1 computes from a set of vectors an AF of greatest significance to the set of vectors. At each stage of the algorithm, SVD is performed for three vectors. Given three non-orthogonal vectors $\boldsymbol{y}_1$, $\boldsymbol{y}_2$, and $\boldsymbol{y}_i$, calculating the 3×3 covariance matrix (Equation 2) formed from these three vectors, Equation 1 is used to replace the input vectors with three AFs equivalent to the three input vectors $\boldsymbol{y}_1$, $\boldsymbol{y}_2$, and $\boldsymbol{y}_i$. There are n-coordinates for each of the vectors $\boldsymbol{y}_1$, $\boldsymbol{y}_2$, and $\boldsymbol{y}_i$. If these n-coordinates from these three vectors are used to define points (a_{j1}, b_{j2}, c_{ji}), a scatter plot of these points provides a graphical interpretation (Figure 3) of the transformation performed for each set of three vectors by the inner loop in Table 1. The transformation matrix (defined by Equation 1) formed from the computed eigenvectors and eigenvalues of the 3×3 covariance matrix (Equation 2) prescribes how to alter the initial scatter plot of points in 3D space to maximize variation in the transformed scatter points in the direction of the coordinate axes (Figure 3). Thus, each step in the inner loop gathers the information contents into three new vectors. The vector $\boldsymbol{y}_1$ is the target of the inner loop, namely, $\boldsymbol{y}_1$ is the approximation to the most significant AF. With each step performed in the inner loop, the position in the list of vectors increments, indicated by the index of $\boldsymbol{y}_i$, from last to first, and the position in the list of vectors for the other two vectors $\boldsymbol{y}_1$and $\boldsymbol{y}_2$ remain constant. The steps performed in the iSVD algorithm are analogous to an insertion sort algorithm, in the sense that after one passes through a list of records, the record with the largest key is placed in the first entry in the table of records. Insertion sort achieves the movement of records to a sorted list of records by comparing for each record, the size of the key. The comparison in the case of insertion sort differs from iSVD in the sense that the values of the key for each record are not modified. In the case of iSVD, the values for the key (eigenvalues) and the records (eigenvectors) alter with each comparison. Nonetheless, changes occur during iSVD that always maintain the movement of information toward obtaining the AF that characterizes the greatest variance within the initial set of vectors.

A single pass through a set of vectors does not yield the exact AF of interest for the following reason. When calculating the most significant AF, the set of vectors is divided into the vector $\boldsymbol{y}_1$and the set of vectors $\{\boldsymbol{y}_2, \ldots, \boldsymbol{y}_m\}$. The steps in Table 1 only ever apply the least squares principle to three vectors at a time. Therefore, one pass through the inner loop cannot, in general, yield a vector with the property required of the most significant AF, namely, orthogonality to the transformed vectors $\{\overline{\boldsymbol{y}}_2, \ldots, \overline{\boldsymbol{y}}_m\}$. The least squares principle applied through forming 3×3 covariance matrices must be repeated multiple times to achieve, on convergence, a new vector $\boldsymbol{u}_1$that is orthogonal to all vectors in the set $\{\overline{\boldsymbol{y}}_2, \ldots, \overline{\boldsymbol{y}}_m\}$.

TABLE 1 Algorithmic steps used to compute the most significant abstract factor (AF) from a set of vectors.

Given a set of vectors $\{\boldsymbol{y}_1, \ldots, \boldsymbol{y}_m\}$

$$\boldsymbol{y}_k = \begin{pmatrix} a_{1k} \\ a_{2k} \\ a_{3k} \\ \vdots \\ \vdots \\ a_{nk} \end{pmatrix}$$

repeat "while current approximation to largest eigenvector has not converged"
loop $i = m$ down to 3 do
"Replace the vectors $\boldsymbol{y}_1$, $\boldsymbol{y}_2$ and $\boldsymbol{y}_i$ by transformed vectors corresponding to the eigenvectors of the covariance matrix computed from $\boldsymbol{y}_1$, $\boldsymbol{y}_2$, and $\boldsymbol{y}_i$ in the order of magnitude of the eigenvalues and return the largest eigenvalue."

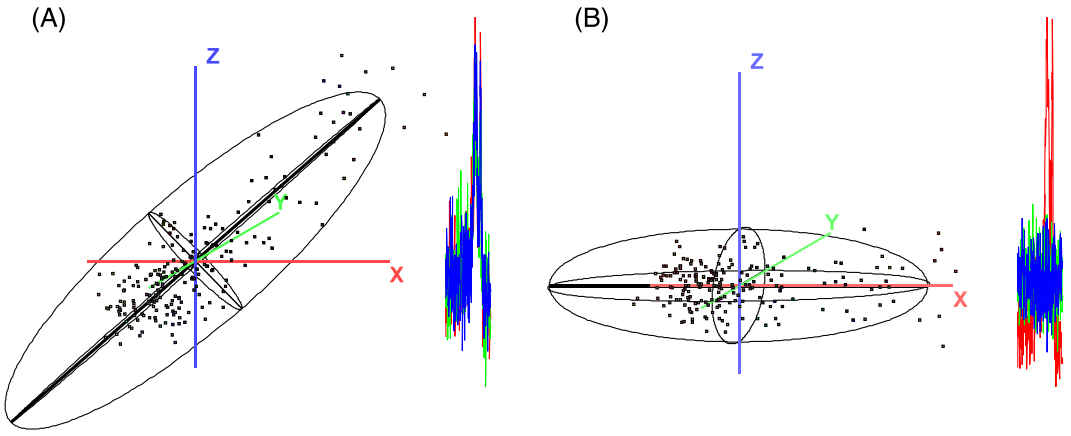

FIGURE 3 (A) Three vectors (in this case derived from spectra with minimal peak structure) displayed with respect to the natural coordinate axes. The elliptical curves are plotted with respect to the principal axes computed for these data points. (B) Three abstract vectors calculated for the 3×3 covariance matrix formed from vectors in (A). The scatter plot formed from AS aligns the variance within the point distribution with the coordinate axes.

2 | CASE STUDY: APPLICATION OF IMAGING XPS TO THE ANALYSIS OF A GOLD WIRE FIXED TO GLASS USING SILVER COATING

2.1 | Sample description

A sample suitable for illustrating aspects of imaging XPS is prepared with a thin gold wire attached to a silicon glass by a silver DAG. The position of the wire on the glass fixed using silver coating at one end of the wire offers three compositionally distinct materials in three spatially separated zones within the analysis area. Stigmatic imaging of the sample is performed using a Kratos Axis Nova imaging analyzer.[19] The measurement proceeds by measuring the signal using a delay line detector configured to discriminate x-, and y-coordinates for the signal detected. The transfer lens system is used to form the total electron image of the sample at the entrance aperture to the mirror hemispherical analyzer which then energy-filters the image formed at the entrance aperture plane to allow an energy-specific image of the sample to form at the detector plane. A set of images is measured corresponding to energies incremented over the interval [600, −5] eV of binding energy. This imaging XPS data set is acquired using 4 s per image. The entire acquisition time for these data is 40.4 min. The maximum count per pixel in all images is 8 counts. Despite these low counts, the imaging data set remains open to analysis.

In spectroscopic terms, by summing the counts in each image and plotting the sum of counts per image against energy, an energy spectrum is obtained. Figure 4A is a spectrum formed from the data set of images shown in Figure 4B. To illustrate in more detail, the lack of signal per image pixel within the imaging data set in Figure 4B, four images from the data set (corresponding to apparent binding energy for Ag 3d photoemission, [371,367] eV) are plotted in Figure 4C. Using PCA noise-reduction (described below), making use of three AFs in the reconstruction of images, the enhancement of signal that results for these four images is shown in Figure 4D. Spatially distinct signals can be discerned within these images, where a low-intensity signal (green) indicates an absence of silver. The intense signal at the top-right-hand corner of Figure 4D is due to emission from the silver coating, while the vertical line of signal in the center of the image is related to the presence of the gold wire. These three zones (Figure 4D) are far less obvious in the raw data (Figure 4C). The PCA processing resulting in these images in Figure 4D is an example of how linear algebra and SVD make it possible to identify spatial information without sacrificing energy information.

2.2 | Calculating AI

The imaging XPS data set illustrated in Figure 4B contains 606 images. Each image contains 16,384 pixels; therefore, when vectors are constructed from spectra, the number of vectors involved when computing AS is also equal to 16,384, but even constructing vectors from images results in 606 vectors. If it were necessary to form the covariance matrix for either 606 images or 16,384 spectra, diagonalization of the covariance matrix through computing all eigenvalues and eigenvectors for the chosen covariance matrix, would render SVD unusable for these data. Fortunately, for imaging XPS data, the number of AFs required to complete an analysis is typically less than 20. Further, iSVD and NIPALS algorithms do not require the computation of all eigenvalues and eigenvectors for the chosen covariance matrix, and so, the excessive time required to compute a full SVD is unnecessary.

Even if we choose to compute a limited number of eigenvalues and eigenvectors, the convergence of iteration schemes such as iSVD and NIPALS is slowed by the numerical precision necessary and the size of the problem posed by the data set in Figure 4B. Hence, an alternative strategy is required for such data sets. One solution is to prefilter the images using iSVD, where the numerical precision required to achieve SVD is relaxed. The sorting properties of iSVD are still active, even when the criteria for terminating the outer loop in Table 1 is relaxed. Therefore, the first step to computing AI is to sort the data set using iSVD, where iSVD performs fewer iterations per cycle for iSVD steps described in Table 1. The precision in each abstract image, so computed, is lower than if SVD was performed correctly, but the sorting achieved by iSVD moves the important information into the newly created AI. Thus, following the prefiltering phase a limited set of AI are calculated that form the input to full precision iSVD. The change in images shown between Figure 4C,D and is achieved by prefiltering the entire data set by computing 20 low-precision AI. High-precision iSVD is applied to these 20 AI to produce the final 20 AI. Three high-precision AI are selected for reconstructing all images in the data set resulting in the quality of images shown in Figure 4D. The information sorting property of iSVD is essential for this approach to computing a limited number of AI.

Application of the prefiltered iSVD algorithm to the data set in Figure 4B yields AI in Figure 5A and AS in Figure 5B. These two sets of AFs calculated from the same data set demonstrate the abstract nature of PCA of spectra, in the sense that, all AS contain shapes that would be considered nonphysical spectral forms. By contrast, AI is more easily interpreted with respect to zones on the sample of different compositions. It is certainly true that on inspection of the AS, it is possible to identify peak patterns that could be viewed as belonging to the glass material (AS 1st). Similarly, AS 2nd and AS 3rd include peaks that could be associated with the silver composite and the gold wire, respectively. However, in spectroscopic terms, neither the first three AI nor the first three AS result in spectroscopic shapes for all spectra-at-pixels reconstructed from three AFs. These nonphysical spectroscopic shapes manifest as negatively inverted peak shapes associated with the Ag 3d signal (Figure 5C). By contrast, the spatial partitioning of information in the AI results immediately offers a means of selecting pixels from which spectroscopic data can be gathered from Figure 4B. That is, AI 2nd in Figure 5A highlights a zone corresponding to silver composite. Similarly, AI 3rd partitions the image into the gold wire and not the gold wire. Thus, classifying pixels by intensity in AI 2nd, then summing spectra-at-pixels for the zone in which silver composite is found, allows a spectrum mostly representative of silver composite to be computed. The complement of the silver composite zone will be a combination of signals from gold wire and glass signal. Similarly, AI 3rd provides the

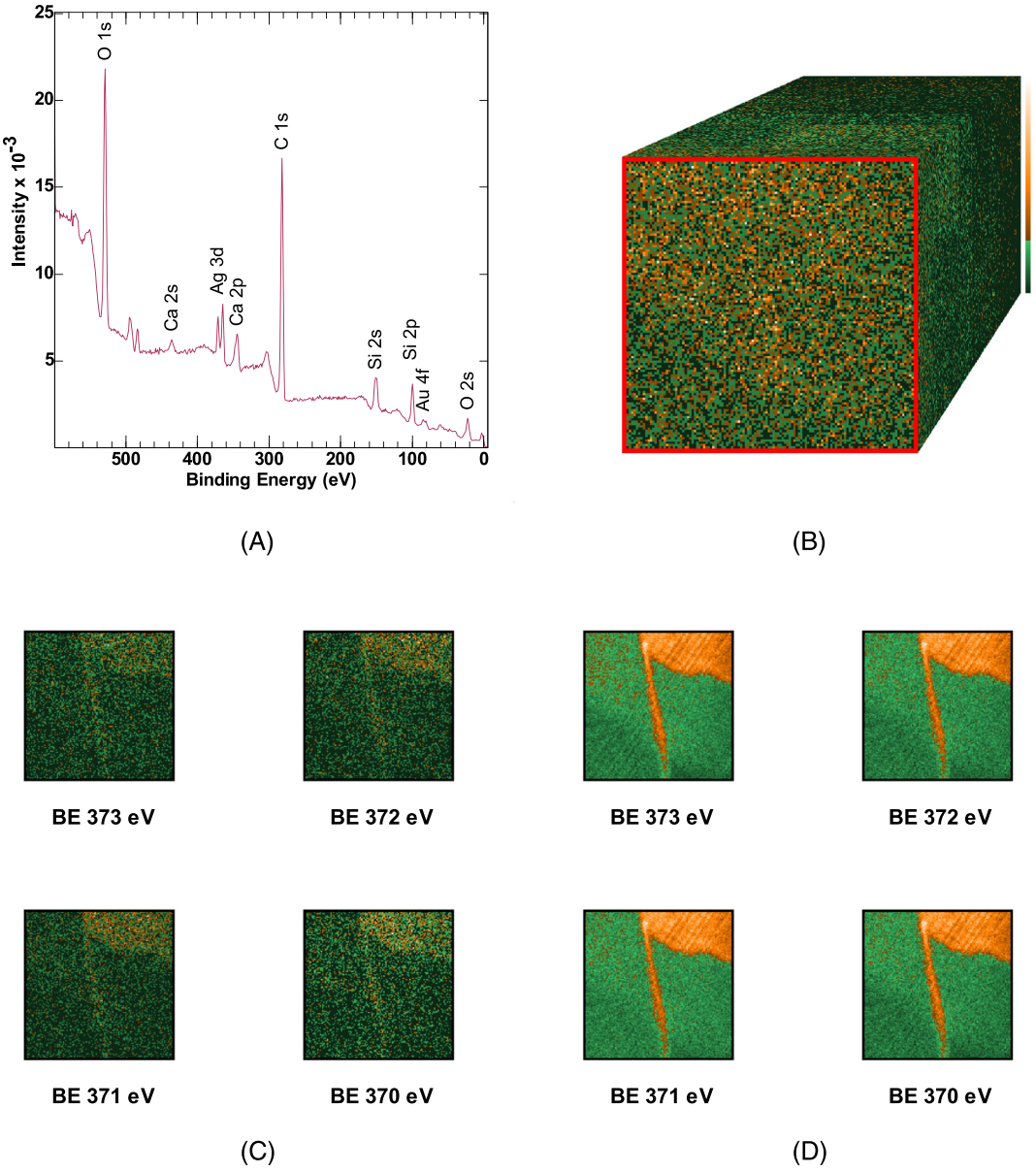

FIGURE 4 (A) Spectrum formed from data bins corresponding to energy at which image data is acquired. The intensity in each data bin of the spectrum is the sum of the signal recorded for an image. (B) Rectangular cuboid formed by plotting the set of images ordered within the display by energy for each image. The spectrum in (A) is calculated from the images in (B). (C) Four unprocessed images were measured with energy corresponding to the photoemission binding energy of Ag 3d. (D) The four images displayed in (C), following the reconstruction of images by fitting the three most significant AI computed from image data displayed in (B).

classification of pixels by intensity, a spectrum mostly originating from the gold wire and a spectrum containing glass and silver composite signals. Hence, the image AFs provide a relatively simple path to obtaining spectra that are readily interpreted.

2.3 | Extracting spectra from images

The simplest way to construct a spectrum from an imaging XPS data set is to integrate signals for each image over the full area of the images and then present these intensities using the energy for images as the independent variable. Figure 4A is an example of a spectrum constructed by this method. However, the spectrum in Figure 4A does not permit a meaningful atomic concentration for the sample in the sense that the elements labeled in Figure 4A are not uniformly distributed over the sample surface. There is no meaningful relationship between silicon, for example, and silver; thus reporting the composition of the sample based on the spectrum Figure 4A does not reflect the three distinct materials that form the sample in question. The spectrum does provide an overview in terms of elements present, but

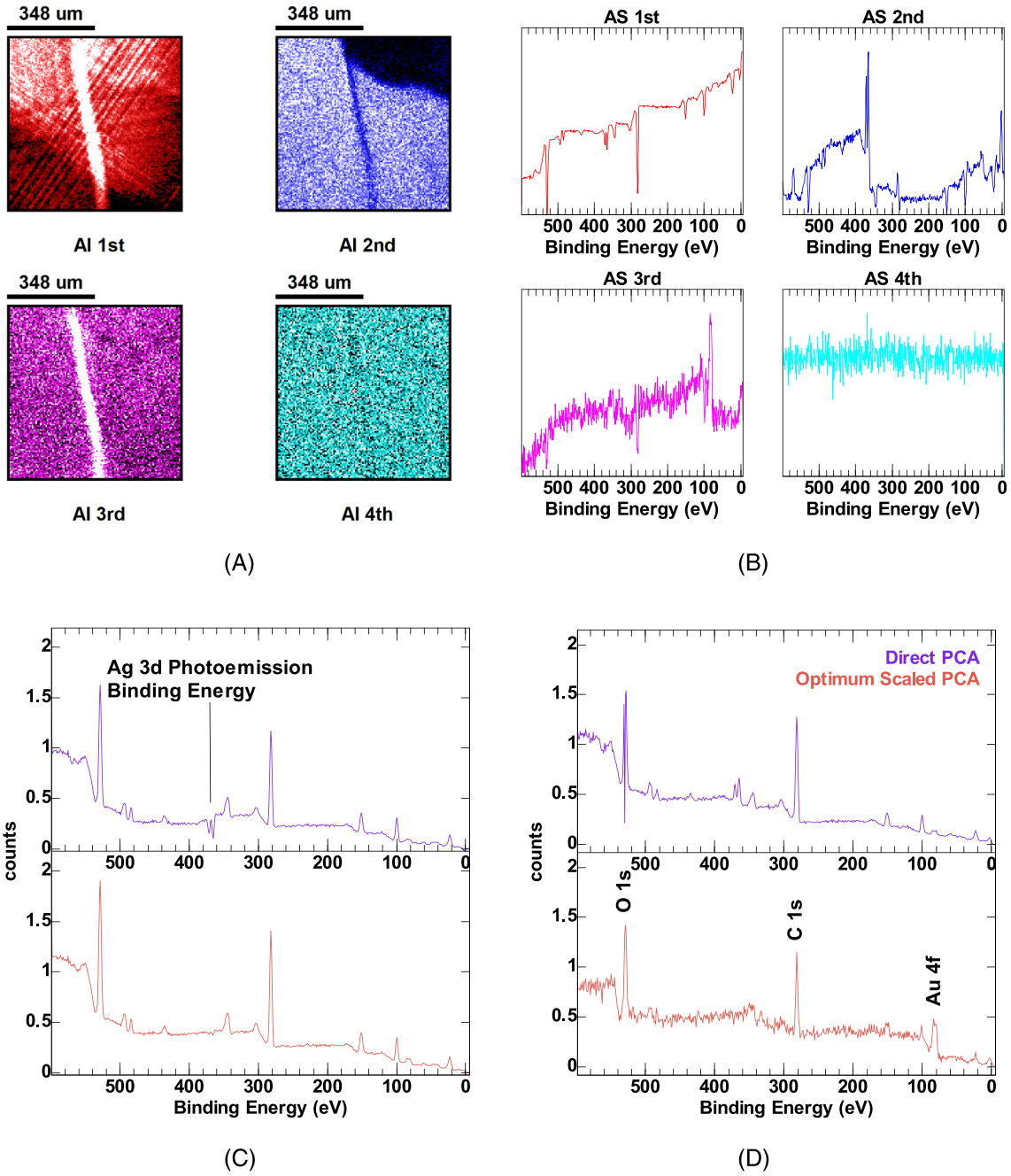

FIGURE 5 (A) The first four abstract images (AI) calculated by iterative SVD (iSVD) applied to image vectors corresponding to the data set in Figure 4B. (B) The first four abstract spectra (AS) calculated by iSVD applied to spectrum vectors corresponding to the data set in Figure 4B. (C) Two examples of PCA-enhanced spectrum-at-pixels spectra. These two pixels are chosen to illustrate the potential for erroneous peak intensities made obvious by the negatively going peak shape corresponding to the Ag 3d signal. These two spectrum-at-pixels spectra were reconstructed from three PCA AFs computed using, so-called, optimum scaling[21–23] preprocessing of image data. (D) Comparison of PCA reconstructed spectrum-at-pixel computed for the pixel (63,58) using PCA without scaling (Direct PCA) and PCA following scaling of data using optimum scaling.[22,23] Note that the spectrum-at-pixel computed by PCA using raw data is predominantly the character of the average spectrum shown in Figure 4A, whereas the spectrum-at-pixel computed using optimal scaling has a pronounced Au 4f peak. In principle, both spectra-at-pixels should be identical for the identical pixel in the imaging XPS data set.

to properly understand the sample, the pixels would be better used by partitioning the imaged area with respect to the locations of these different materials.

Classifying pixel locations according to intensity offers a means of constructing spectra from imaging XPS data sets that correspond to zones for which the composition is more homogeneous than the

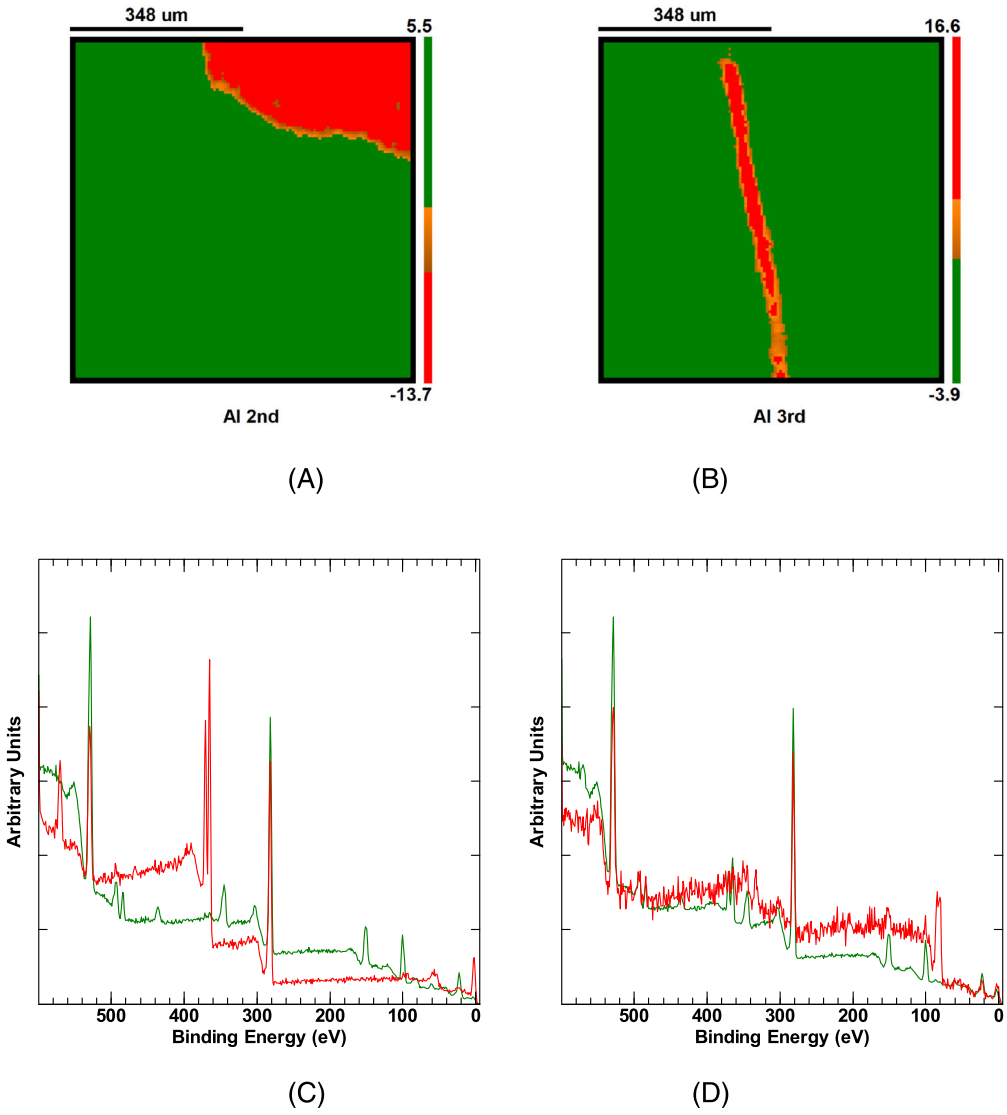

FIGURE 6 Classification of Al 2nd and Al 3rd images using intensity to assign two colors highlighting (A) the silver composite in Al 2nd and (B) the gold wire in Al 3rd. Spectra computed by summing spectra-at-pixels with common color assignment in (A) and (B) are displayed in (C) and (D), respectively.

sample taken as a whole. The images and spectra in Figure 6 are examples where the images are classified into two zones per image, and from these two zones marked up using red and green colors, for each image, two spectra are calculated from the data set illustrated in Figure 4B. These four spectra shown in Figure 6C,D are true spectra in the same sense as the spectrum in Figure 4A. These spectra may not fully represent the individual zones required to characterize glass, silver composite, and gold wire, but from these spectra, component spectra representative of glass, silver composite, and gold wire can be constructed.

One advantage of imaging XPS data is that spectra from zones with different proportions of the sample chemistry can be obtained in the same way that spectra in Figure 6 relate to the colored pixels in the two images. All that is required is to make a different classification of pixels, of which the rectangular zone shown in Figure 7B is an example. It is therefore possible to test component spectra by fitting component spectra to spectra, such as the spectrum in Figure 7A. Figure 7A is an example of fitting three component spectra to a spectrum using LLS optimization.[19] The quality of the fit of these component spectra to data is measured through the residual standard deviation statistic and the uniformity of the residual plot. The rectangular zone (Figure 7B) includes a significant proportion of the gold wire but also includes pixels corresponding to the silver composite and the glass. Hence, all three component spectra are required to fit the spectrum shown in Figure 7A.

The value of constructing three component spectra lies in obtaining spectral shapes that can be interpreted using conventional quantification of XPS spectra. By way of example, the component spectrum corresponding to silver composite is displayed in Figure 7C, where a quantification table based on integration regions is displayed over the data. The ability to separate a spectrum into component spectra for which quantification is possible provides a deeper insight into sample chemistry than would be possible if the total spectrum in Figure 4A was the only spectrum available. Indeed, imaging XPS data sets are a source for spectra in a variety of forms, all of which can be used to test the validity of the hypothesis that the three component spectra in Figure 7A are physically meaningful.

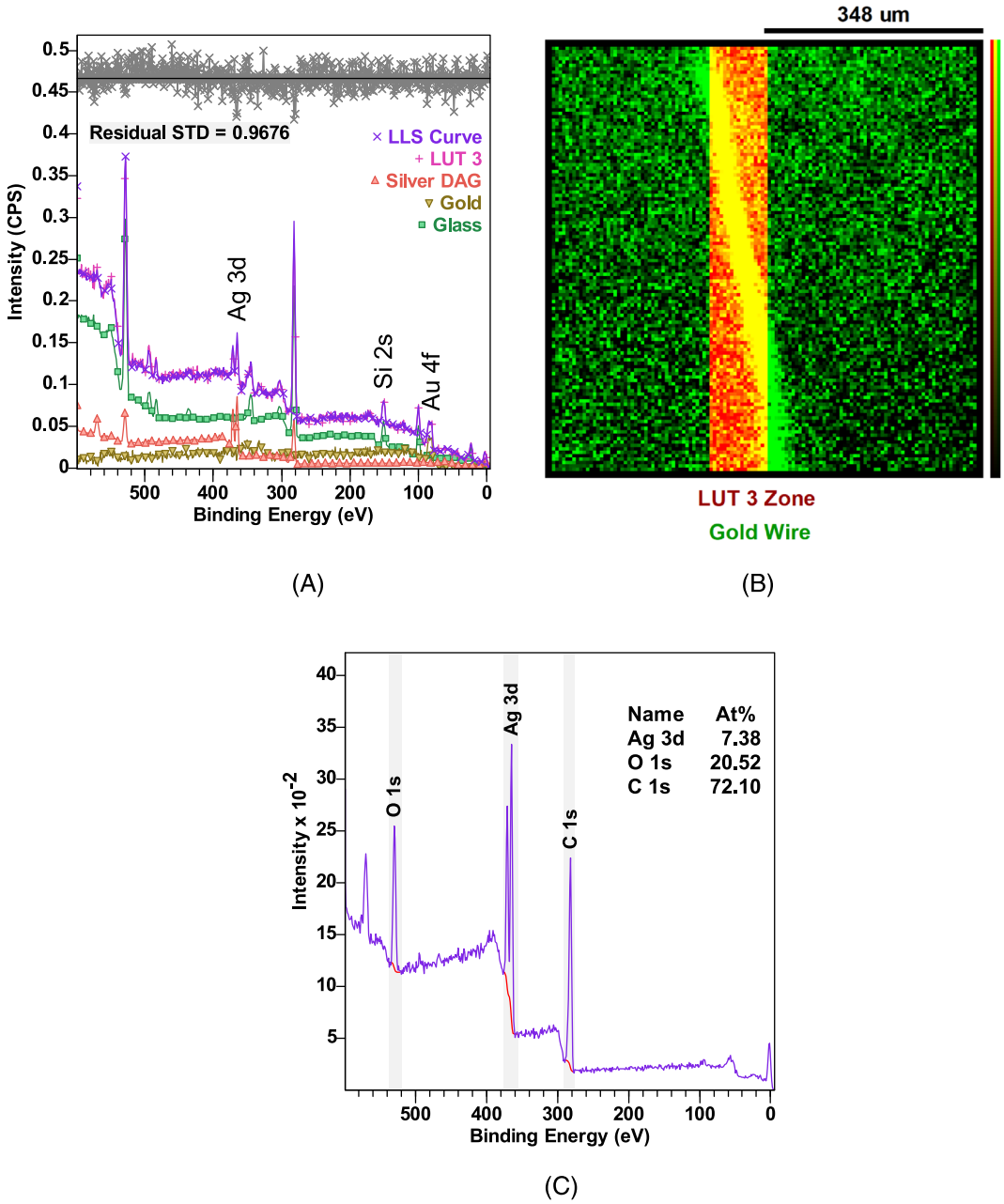

FIGURE 7 (A) Lookup table (LUT) spectrum constructed from the data set in Figure 7B using only pixels within the rectangle shown in (B). The spectrum is decomposed into three component spectra calculated from the spectra displayed in Figure 6. (B) LUT zone overlaid on an image of the gold wire. Only pixels within the rectangle marked in red and yellow are used to sum spectra-at-pixels from the data set Figure 4B to form the spectrum in (A). (C) Component spectrum gathered from the location of the silver composite used to fix the gold wire to glass.

2.4 | Data scaling

For the described sample, preprocessing of data in preparation for PCA can be shown to be important. Attempting to identify pixels corresponding to the location of the gold wire is susceptible to low signal-to-noise and the scarcity of pixels within the gold domain compared to glass or silver composite domains. If PCA is applied to raw image data, only two AI are distinct from noise. Only when data are scaled using optimum scaling[21–23] are the three AI shown in Figure 5A apparent. Moreover, if noise reduction is performed using PCA applied to raw data and if two AI are used in the reconstruction step that enhances signal-to-noise, then the spectra-at-pixels fail to include a contribution in the form of varying Au 4f signal (Figure 5D). Hence, a direct application of PCA to raw imaging XPS data may fail to characterize a thin gold wire on a sample. For this reason, it is always advisable to experiment with scaling options available to PCA for imaging XPS data sets.[21] It is also advisable to construct spectra by summation of raw spectra-at-pixels. If PCA is applied to produce AI and pixel intensities are classified into zones corresponding to physically different domains, then constructing spectra directly from

raw imaging XPS data ensures that artifacts within spectroscopic data due to PCA are eliminated. This point should be emphasized by reiterating that the spectra in Figure 6C,D are examples of spectra computed directly from imaging XPS raw data and are therefore without artifacts that otherwise appear due to data processing, such as those evidenced in Figure 5D.

3 | SUMMARY

Linear algebra and more direct methods for computing spectra from imaging XPS are described. The role of data scaling in the analysis of imaging XPS is demonstrated to be important when working with low signal-to-noise data. A case study of imaging XPS applied to a sample with three domains of different compositions is used to demonstrate the use of these methods to recover spectroscopic data from distinct sample domains. The imaging XPS methods described here are especially applicable to a broad field of materials including conventional and electrochemical catalysts where spatial sample composition dependence is important and evolves with time and reaction conditions.

AUTHOR CONTRIBUTIONS

Vincent Fernandez: Investigation (lead); writing—review and editing (equal). **Neal Fairley**: Conceptualization (lead); investigation (supporting); methodology (lead); writing—original draft (equal); writing—review and editing (equal). **Pascal Bargiela**: Investigation (lead); writing—review and editing (equal). **David Morgan**: Methodology (supporting); writing—review and editing (equal). **Jonas Baltrusaitis**: Conceptualization (supporting); methodology (supporting); supervision (lead); writing—original draft (equal); writing—review and editing (equal).

ACKNOWLEDGEMENTS

This work by JB was supported as part of Understanding & Controlling Accelerated and Gradual Evolution of Materials for Energy (UNCAGE-ME), an Energy Frontier Research Center funded by the U.S. Department of Energy, Office of Science, Basic Energy Sciences under Award # DE-SC0012577. The CNRS is acknowledged for financial support to the Thematic Workshop (N° 1317144) held at the Station Biologique, Roscoff, France. We also acknowledge Michelle Fairley for contributing to the creation of Figure 1.

CONFLICT OF INTEREST STATEMENT

The authors declare no competing interests.

DATA AVAILABILITY STATEMENT

Available upon request.

ORCID

David Morgan https://orcid.org/0000-0002-6571-5731
Jonas Baltrusaitis https://orcid.org/0000-0001-5634-955X

REFERENCES

1. Ian W. Drummond, XPS: Instrumentation and Performance. In: Briggs D, Grant JT, eds. *Surf. Anal. By auger X-ray photoelectron Spectrosc*. IMPublications, Chichester, UK and SurfaceSpectra; 2003:899.
2. Shard AG. Practical guides for x-ray photoelectron spectroscopy: quantitative XPS. *J Vac Sci Technol a*. 2020;38(4):041201. doi:10.1116/1.5141395
3. Fernandez V, Renault O, Fairley N, Baltrusaitis J. Surface science insight note: optimizing XPS instrument performance for quantification of spectra. *Surf Interface Anal*. 2024; 1–11. doi:10.1002/sia.7296
4. Morgan DJ. Imaging XPS for industrial applications. *J Electron Spectros Relat Phenomena*. 2019;231:109-117. doi:10.1016/j.elspec.2017.12.008
5. Golub GH, Reinsch C. Singular value decomposition and least squares solutions. *Numer Math*. 1970;14(5):403-420. doi:10.1007/BF02163027
6. Fernandez V, Morgan D, Bargiela P, Fairley N, Baltrusaitis J. Combining PCA and nonlinear fitting of peak models to re-evaluate C 1s XPS spectrum of cellulose. *Appl Surf Sci*. 2023;614:156182. doi:10.1016/j.apsusc.2022.156182
7. Fairley N, Bargiela P, Huang W-M, Baltrusaitis J. Principal component analysis (PCA) unravels spectral components present in XPS spectra of complex oxide films on iron foil. *Appl Surf Sci Adv*. 2023;17:100447. doi:10.1016/j.apsadv.2023.100447
8. Siegbahn G. Electron spectroscopy for chemical analysis (e.s.c.a.). *Philos Trans R Soc London Ser a, Math Phys Sci*. 1970;268:33-57. doi:10.1098/rsta.1970.0060
9. Walton J, Fairley N. Quantitative surface chemical-state microscopy by x-ray photoelectron spectroscopy. *Surf Interface Anal*. 2004;36(1):89-91. doi:10.1002/sia.1654
10. Walton J, Fairley N. XPS spectromicroscopy: exploiting the relationship between images and spectra. *Surf Interface Anal*. 2008;40(3-4):478-481. doi:10.1002/sia.2731
11. Walton J, Fairley N. Characterisation of the Kratos Axis ultra with spherical mirror analyser for XPS imaging. *Surf Interface Anal*. 2006;38(8):1230-1235. doi:10.1002/sia.2381
12. Walton J, Fairley N. Transmission-function correction for XPS spectrum imaging. *Surf Interface Anal*. 2006;38(4):388-391. doi:10.1002/sia.2131
13. Smith EF, Briggs D, Fairley N. Further developments in quantitative X-ray photoelectron spectromicroscopy: preliminary results from the study of germanium corrosion. *Surf Interface Anal*. 2006;38(2):69-75. doi:10.1002/sia.2199
14. Hajati S, Tougaard S, Walton J, Fairley N. Noise reduction procedures applied to XPS imaging of depth distribution of atoms on the nanoscale. *Surf Sci*. 2008;602(18):3064-3070. doi:10.1016/j.susc.2008.08.005
15. Fairley N, Fernandez V, Richard-Plouet M, et al. Systematic and collaborative approach to problem solving using X-ray photoelectron spectroscopy. *Appl Surf Sci Adv*. 2021;5:100112. doi:10.1016/j.apsadv.2021.100112
16. Malinowski ER. *Factor analysis in chemistry*. 3rd ed. John Wiley & Sons, Ltd; 2002.
17. Walton J, Fairley N. Noise reduction in X-ray photoelectron spectromicroscopy by a singular value decomposition sorting procedure. *J Electron Spectros Relat Phenomena*. 2005;148(1):29-40. doi:10.1016/j.elspec.2005.02.003
18. Béchu S, Richard-Plouet M, Fernandez V, Walton J, Fairley N. Developments in numerical treatments for large data sets of XPS images. *Surf Interface Anal*. 2016;48(5):301-309. doi:10.1002/sia.5970
19. Bauer FL, Householder AS, Wilkinson JH, Reinsch C. *Handbook for automatic computation: volume II: linear algebra*. Springer; 2012.
20. Marquardt DW. An algorithm for least-squares estimation of nonlinear parameters. *J Soc Ind Appl Math*. 1963;11(2):431-441. doi:10.1137/0111030

21. Walton J, Fairley N. Data scaling for quantitative imaging XPS. *Surf Interface Anal*. 2009;41(2):114-118. doi:10.1002/sia.2974
22. Keenan MR, Kotula PG. Optimal scaling of TOF-SIMS spectrum-images prior to multivariate statistical analysis. *Appl Surf Sci*. 2004; 231–232:240-244. doi:10.1016/j.apsusc.2004.03.025
23. Keenan MR, Kotula PG. Accounting for Poisson noise in the multivariate analysis of ToF-SIMS spectrum images. *Surf Interface Anal*. 2004; 36(3):203-212. doi:10.1002/sia.1657

How to cite this article: Fernandez V, Fairley N, Morgan D, Bargiela P, Baltrusaitis J. Surface science insight note: Imaging X-ray photoelectron spectroscopy. *Surf Interface Anal*. 2024; 1-12. doi:10.1002/sia.7337